P-ISSN: 2798-1134 | E-ISSN: 2797-3549 | DOI: 10.52562/injoes.2023.632

Indonesian Journal of Earth Sciences

https://journal.moripublishing.com/index.php/injoes

| Research Article |

Contribution of ALOS PALSAR DEM Imagery to the Study of Geological and Morphostructural Lineaments of Boma Trough Block, Onshore Coastal Basin of D.R. Congo

Shams Mbudi Diambu[1,3,5*], Dominique Wetshondo Osomba[2,3], Thomas Kanika Mayena[2], Clement N'zau Umba-di-Mbudi[2,4]

[1] *Department of Exploration and Production, Faculty of Oil, Gas and Renewable Energies, University of Kinshasa, Kinshasa, D.R. Congo*
[2] *Department of Geosciences, Faculty of Sciences and Technologies, University of Kinshasa, Kinshasa, D.R. Congo*
[3] *Mining and Petroleum Resources Engineering (GeReMiPe), Laboratory, University of Kinshasa, Kinshasa, D.R. Congo*
[4] *Polytechnic Faculty, President Joseph Kasa-Vubu State University, Boma, D.R. Congo*
[5] *Department of Geology, National Geological Service of Congo, Kinshasa, D.R. Congo*
** Correspondence: shams.mbudi@unikin.ac.cd*

Received: 11 May 2023 / Accepted: 06 June 2023 / Published: 11 June 2023

Abstract: Geological and morphostructural lineaments are considered as the surface expression of geological structures and linear features of valleys, ridges and river drainage systems. Lineaments extracted from satellite images have always been effective in understanding the structural context of a region. The lineaments observed on the surface provide information on the tectonic stresses that have affected an area and give a first impression of the probable existence and orientation of geological structures that may constitute oil traps at depth. This study aims to semi-automatically extract lineaments (by combining the use of GIS software, remote sensing and operator intervention) in Boma Trough Block, an oil block located to the east of D.R. Congo Coastal Basin and still poorly explored. The satellite image used in this work is an ALOS PALSAR DEM with a spatial resolution of 12.5m, enhanced in traditional hillshade (solar azimuth of 315° and 45°) and multidirectional hillshade; which allowed the extraction of 3129 lineaments, with lengths ranging from 0.16 to 3.79 km, oriented on multidirectional hillshade at 47.1% along the NW-SE direction, at 44.1% along the NE-SW, 7.3% for N-S and 1.4% for E-W. Lineament density mapping revealed that areas with high and very high densities cover 43% of the study area, where the Precambrian basement is largely outcropping, while low and very low density areas represent 41% and contain sedimentary formations. Areas with moderate densities covered 16%. The lineaments extracted from the DEM image compared to the reality on the field show a positive correlation. This confirms the important contribution of the processing approach used in this study.

Keywords: Lineament, Boma Trough Block, ALOS PALSAR DEM, Hillshade image, Semi-automatic extraction

INTRODUCTION

Linear elements on the earth's surface have always attracted the attention of geologists, who have proven that lineaments seen in remote sensing images are reliable indicators of the geological structures of a region (Scanvic, 1983). The term "lineament" was originally proposed to refer to significant lines in the landscape caused by fractures and faults related to the basement architecture (Hobbs, 1904).

According to their genesis, Echeverria et al. (2022) distinguish three types of lineaments: (i) geological, (ii) morphostructural and (iii) non-geological. Geological lineaments are mappable linear surfaces that are typically thought of as an expression of discontinuities in geological formations like faults, fractures, joints, or lithological borders (Minár & Sládek, 2009). Morphostructural or topographic lineaments are those created by geomorphological processes. They correspond to the linear features of valleys, river drainage systems and ridges (O'leary et al., 1976). Morphostructural lineaments can have a good equivalence with tectonic structures like faults and fractures (Pal et al., 2006). Non-geological lineaments are those created by human activity, such as roads, railways, boundaries of cultivated fields or any changes in land use patterns (Ahmadi & Pekkan, 2021).

Therefore, it is possible to map terrain features by using remote sensing and geomatics techniques to structurally analyze the earth's surface (Lu & An, 1999). This facilitates obtaining structural and

geological information on large or difficult to access areas through remote sensing data, Geographic Information Systems (GIS) and database management (Guoan, 2014).

In oil research, the lineaments mapped on the surface can provide the first information on the types of tectonic stresses that have affected a region, on the favorable zones for oil seepage on the surface (through faults and fractures for example), on the probable presence and orientation of geological structures that could constitute oil traps at depth. This information can be confirmed and completed later by geological and geophysical work.

Boma Trough is one of the oil blocks of the D.R. Congo Coastal Basin in pre-exploratory phase since its creation in 2011 by the Ministry of Hydrocarbons. This block, with an area of approximately 747 km^2 and located at the western limit of the basin, next to the oil blocks (Mavuma, Losthi and Ndunda) which are subject to exploration licenses, but has never been attributed to the Oil Operators and has not been selected among the 27 blocks included in the Calls for Tenders recently launched by the Congolese Government, because of its geological aspect which is still poorly known (unexplored block) and complex (containing sedimentary rocks and Precambrian basement).

It should also be noted that since the colonial times, several geological mapping works have been carried out around Boma, including the famous works of Lepersonne (1974), Kalala-Ntumba et al. (1975), and Giresse (1982). These works, dating for the most part from about half a century, were carried out using old mapping methods and did not aim to specially study the geological aspect of Boma Trough Block, which was not delimited at the time. This work aims to analyze the geological and morphostructural lineaments of Boma Trough Block, from a DEM (Digital Elevation Model) image of ALOS PALSAR satellite of JAXA (Japan Aerospace Exploration Agency), using some remote sensing and Geographic Information Systems (GIS) software, by comparing the results found with the realities on the field and interpreting them in relation to some previous work.

The choice of this image is justified by the fact that the use of DEM images in general and those resulting from RADAR data in particular (such as ALOS PALSAR DEM) as input data in lineament detection, allows to extract only lineaments based on natural topographic information. Data corresponding to artificial features such as streets, canals, field boundaries, etc., do not appear when obtaining lineaments (Prasad, 2013). In addition, the spatial resolution of the ALOS PALSAR DEM image used is 12.5 meters, equivalent to the size of the smallest element that can be distinguished in this image. This is practically interesting because it allows to better distinguish the lineaments during the extraction process and to detect as many lineaments as possible.

Indeed, automatic extraction generates many lineaments in a short time, but it still has drawbacks because the extracted lines do not always correspond to the geological structures of the studied area (Echeverria et al., 2022). To obtain much more reliable results, we proceeded by a semi-automatic extraction, reworking some automatically extracted lineaments to better match them to the field realities.

STUDY AREA

Location

Located to the east of D.R. Congo Coastal Basin, between 12°45'25.2" East-5°26'45.8" South and 13°12'10.7" East-5°57'1.6" South, the Boma Trough Block extends from the Congo River in the south to the limit of the Mavuma oil sands block in the north, and is included between the Precambrian basement in the east and the Ndunda block in the west.

Figure 1 shows the division into oil blocks of the Coastal Basin of the DR Congo recently mapped by the Ministry of Hydrocarbons and we locate the Boma Trough Block in the southeast with a blue outline.

Geological and structural context

Considering its geographical situation, the geology of Boma Trough Block is similar to the geology of the western part of the Kongo Central province where it is located. By analyzing geological maps at 1/2,000,000 of Zaïre (Lepersonne, 1974), 1/25,000 of Boma (Kalala-Ntumba et al., 1975), 1/2,500,000 of the D.R. Congo (MRAC, 2005) and 1/500,000 of the Kongo Central province (MRAC, 2010), we can note the presence of the following geological formations in Boma Trough Block:

- The Precambrian basement (Zadinian): Composed of magmatic and metamorphic formations (granites, basalts, gneisses, micaschists, migmatites, amphibolites, quartzites, etc.);
- Sedimentary rocks: composed of sublittoral sandstones from the Mesozoic (Cretaceous), marine calcareous rocks from the Phanerozoic, the series of cirques from the Paleocene and Pliocene, recent alluvium and clayey silts from the Quaternary (Holocene).

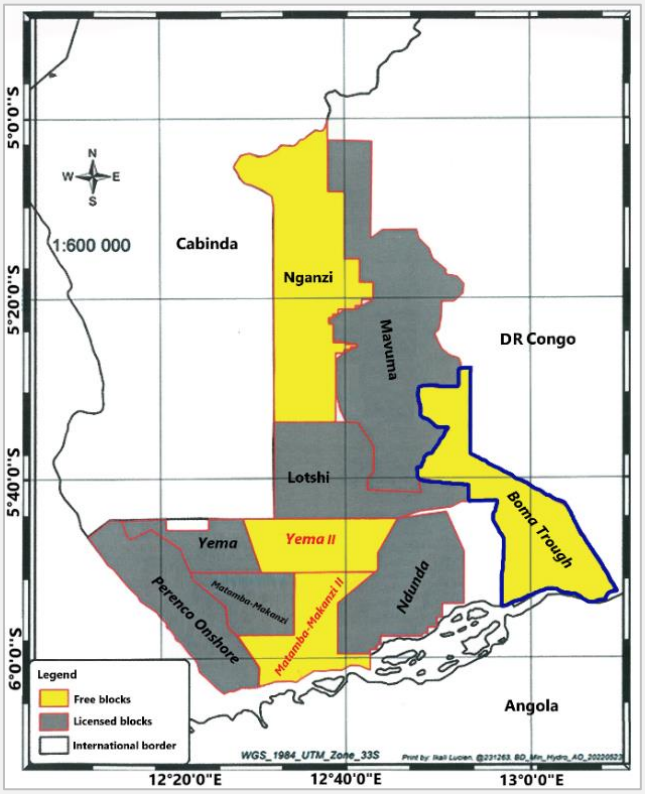

Figure 1. Location of the Boma Trough Block in the Coastal Basin of D.R. Congo (Ministry of Hydrocarbons-General Secretariat, 2022)

Regarding its structural aspect, the western part of the internal domain of Coastal Basin is collapsed and covered by Cretaceous, Tertiary and Quaternary terrains (Giresse, 1982). Near the reliefs of Mayombe, the phenomena of distensions are still clear and lead to the collapse of panels parallel to the direction of the base (NW-SE), which allowed to protect various Senonian deposits from erosion, in particular Maastrichtian phosphates. The current valleys were established in these depressions.

The structure of the post-salt layers is generally considered to be monoclinal with a slight dip towards the ocean. Recent reflection (Air-Gun) seismic surveys conducted over the continental plateau have shown two different types of structures, which are not seen in large-scale deep seismic surveys for oil exploration (Jansen et al., 1984):

- On the inner border, moderate et fairly dense folds, a kind of undulation, affect the Upper Cretaceous and Paleogene together, to Middle Eocene. A significant difference in orientation is visible between the Paleogene folds (N90° to N100°) and the Cretaceous folds (N110° to N120°);
- On the outer border, the Miocene layers are monoclinal and discordant.

The following chronology of events is proposed:

- From the beginning of the Paleocene, a compressive tectonic, probably very moderate, is set up; it is also known in the Bénoué chain at the end of the Cretaceous (Benkhelil & Guiraud, 1980) and seems to correspond to the beginning of a phase of change in the speed of oceanic expansion in South Atlantic (Le Pichon, 1968);
- In the Lutetian, the compression reached its paroxysm as a distant consequence of the Pyrenean-Atlantic phase generated by the rotation of the African plate. This phenomenon is quite general in West and North Africa (Bellion & Guiraud, 1980);
- In the Miocene, a distensive regime reappears according to a new dynamic of the African plate which is oriented towards the North and the beginning of a new phase of oceanic expansion (Le Pichon, 1968).

Based on the geological maps mentioned above, we have elaborated using the ArcGIS 10.8 software, the geological map of Boma Trough Block as presented in Figure 2 below.

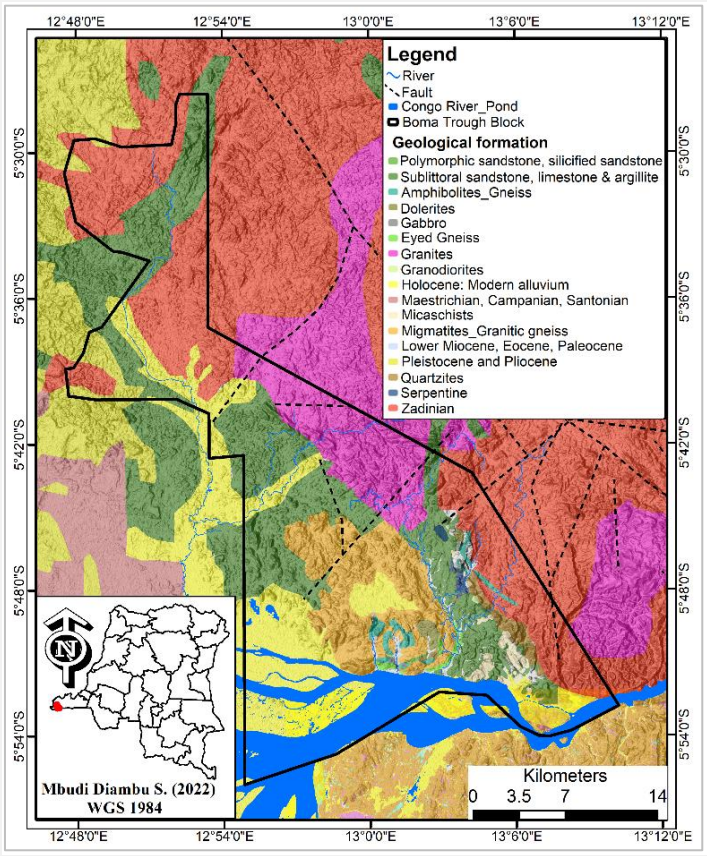

Figure 2. Geological map of the Boma Trough Block

METHOD

Figure 3 below presents a schematic diagram of the methods used to carry out this work. It includes three (3) main steps with the names of the data processing software used: (i) Data collection, (ii) Results, (iii) Discussion.

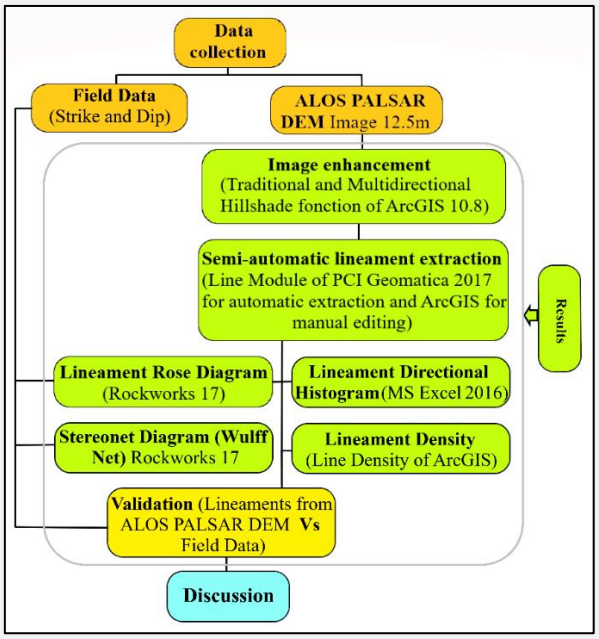

Figure 3. Schematic representation of the method used

DATA COLLECTION

DEM Image used

There are many Digital Elevation Model (DEM) data easily accessible and downloadable from the internet, among which Aziz & Rashwan (2022) mentioned SRTM, ASTER, GDEM, ALOS PALSAR DEM, NASADEM and GTOPO30 data. These images have different spatial resolutions, varying from 12.5 to 1000 meters.

In order to map geological lineaments in our study area, we used DEM data from the satellite ALOS PALSAR (Advanced Land Observing Satellite-Phased Array type L-band Synthetic Aperture Radar) of the Japanese Aerospace Exploration Agency (JAXA). JAXA launched ALOS PALSAR in 2006 and it was operational until May 12, 2011 (Khal et al. 2020). The data obtained from this satellite is used for mapping, observing the use of natural resources and for scientific research.

The ALOS PALSAR DEM image (Figure 4) used in this work has a spatial resolution of 12.5 m, freely downloaded from the Alaska Satellite Facility (ASF) website. Two ALOS PALSAR DEM images mosaicked using the ArcGIS Mosaic to New Raster tool, were needed to cover the study area; these are the AP_08574_FBD_F7060_RT1.dem and AP_08574_FBD_F7070_RT1.dem.

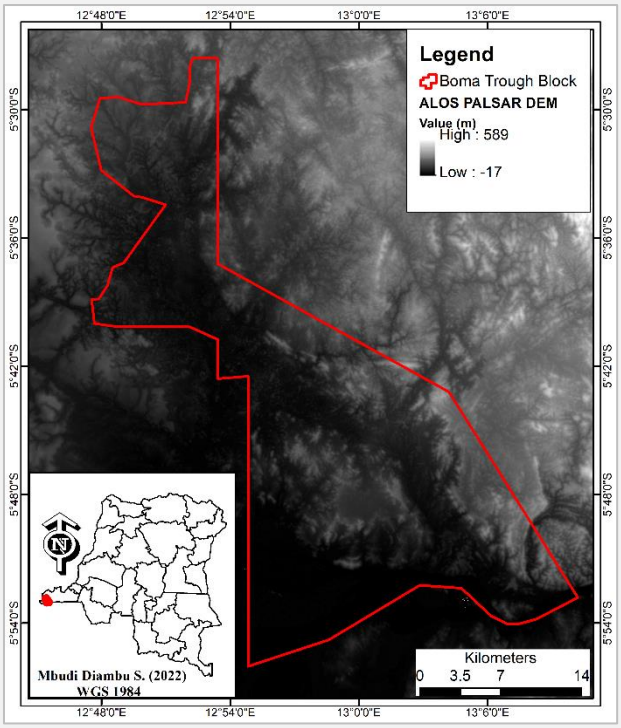

Figure 4. ALOS PALSAR DEM Image used

Field Data

The data collected in the field include structural measurements (strike and dip) of the geological and morphostructural lineaments. The materials used for this purpose are: a Garmin GPS (for the measurement of geographical coordinates of the observation sites of the lineaments), a geologist's compass (for taking structural measurements of the lineaments), a camera (for photographing some interesting facts on the field), a field notebook (for taking notes).

RESULTS

Image enhancement

Enhancement consists of processing an image so that the result is more appropriate than the original image for a specific remote sensing application. Satellite image enhancement techniques offer many choices for improving the visual quality of remote sensing images (Ablin et al., 2020).

During the last decade, digital image processing techniques have been developed to display DEMs as shaded relief images. In the case of DEMs, shaded relief images and terrain-derived products have largely demonstrated their usefulness for lineament and fault mapping (Masoud & Koike, 2011).

The ArcGIS hillshade tool used in this work creates a shaded relief raster from a DEM raster. The DEM contains all the 3D information about the terrain, but it doesn't look like a 3D object. To get a better expression of the terrain, it is possible to calculate a hillshade, which is a raster format with a 3D looking image. The shading is a hypothetical illumination of a surface based on a given azimuth and altitude for the sun. It creates a 3D effect that gives a sense of visual relief to the terrain and is considered the most common way to visualize texture. The use of shade improves the topography of the landscape (William, 2018).

The ArcGIS hillshade feature provides two options for generating hillshades: traditional and multidirectional. The traditional method calculates the shading using a light source in one direction using the elevation properties (angle of the light source above the horizon, 45° by default) and azimuth (angular direction of the sun, measured from north in degrees clockwise from 0 to 360, 315° by default) to specify the position of the sun. The multidirectional method combines light from multiple sources to represent the shaded terrain. By default, shadow and light are shades of gray associated with numbers from 0 to 255 (ascending from black to white) (Nagi, 2014).

In July 2014, ESRI (Environmental Systems Research Institute) launched a new generation of shaded relief, the Multidirectional shaded relief service. This shading was inspired by the work of legendary Swiss artist and cartographer Eduard Imhof. Multidirectional shading provides an excellent representation of world topography and a perfect relief background (Nagi, 2014).

We produced from the ALOS PALSAR DEM image, three shaded reliefs, two (Figure 5) from the traditional method (with the sun positioned at 45° of altitude, azimuths 315° and 45°) and one another from the multidirectional method (Figure 6).

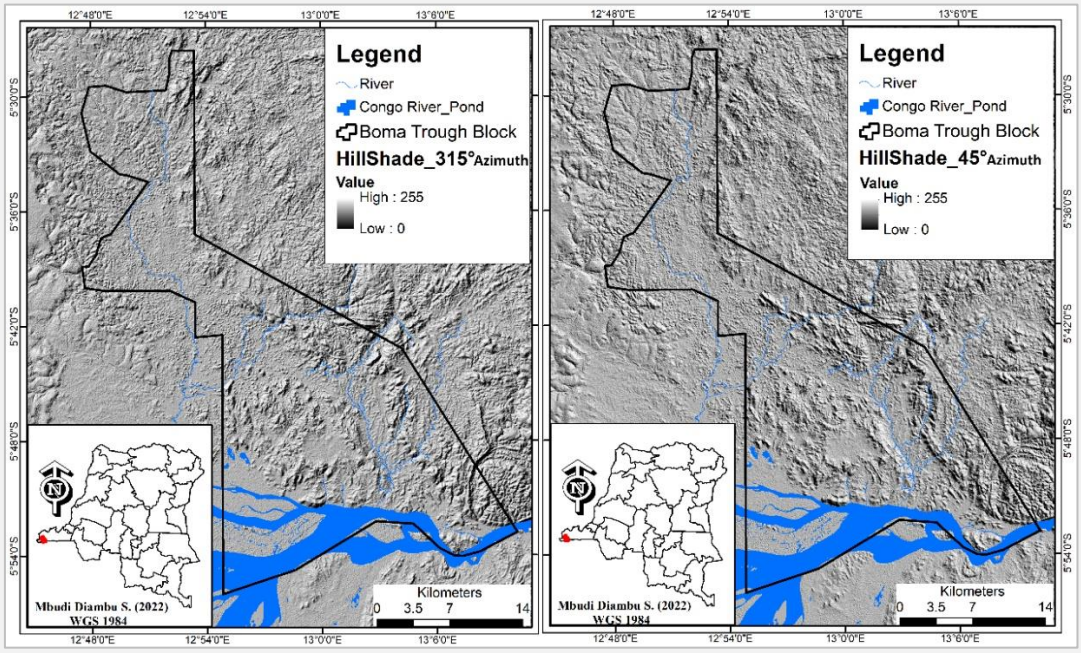

Figure 5. Traditional Hillshade (Azimuths 315° and 45°) of ALOS PALSAR DEM

Extraction of lineaments

The objective of extraction is the digitization of all lineaments in the study area from the hillshade images. Ahmadi & Pekkan (2021) distinguish three methods of lineament extraction:

- Manual extraction: applied when the main objective is to detect geological features (Das et al., 2018). It is performed with visual interpretation and manual digitization of lineaments by human operators (Scheiber et al., 2015);
- The semi-automatic extraction is carried out by analyzing digital images through a first automated process (the detection and extraction of lineaments) and a second phase which corresponds to the interpretation and addition of the lineaments detected by an operator because after lineament extraction, manual editing is required to obtain a complete and correct set of linear features (Suzen & Toprak, 1998);

- Automatic lineament extraction is performed by analyzing digital images using computer software. This automated processing includes the use of various algorithms for image enhancement, filtering and edge detection (Echeverria et al., 2022).

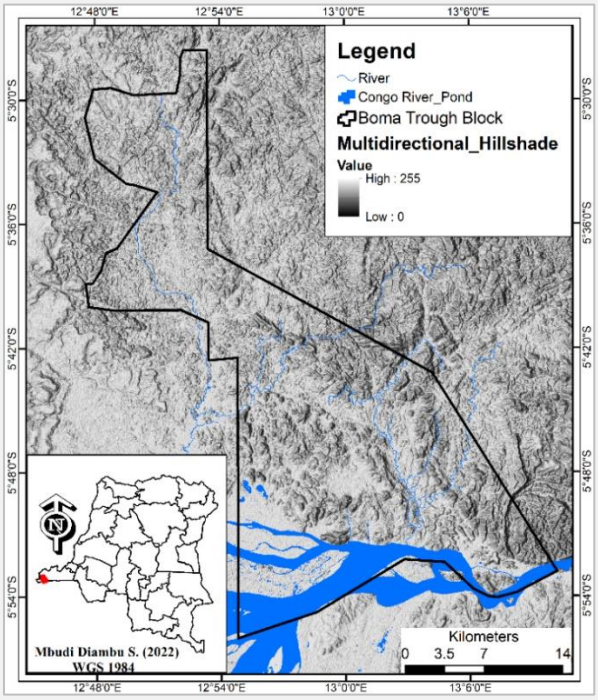

Figure 6. Multidirectional hillshade of ALOS PALSAR DEM

After various extraction tests using the three methods mentioned above, we have chosen the semi-automatic extraction of the lineaments. This method begins with an automated extraction (which allows to extract a lot of lineaments in a short time) and ends with some manual editing by the operator.

The automated extraction step was carried out using the Line Module of the PCI Geomatica 2017 software, which is a module often used for the automatic extraction of lineaments (Salui, 2018). There are two categories of parameters in this module (Table 1): the first category controls the edge detection step, the second detects and extracts curves (Ustinov et al., 2022).

Table 1. Parameters used for the PCI Geomatica Line module (Ustinov et al., 2022)

Parameters	Description	Range and Unit
	Edge Detection	
RADI	Filter Radius. It specifies the radius of the edge detection filter (Filter of Canny).	0–8192 (pixel)
GTHR	Gradient Threshold. It specifies the threshold for the minimum gradient level for an edge pixel to obtain a binary image (Filter of Canny).	0–255
	Curve extraction	
LTHR	Length Threshold: It specifies the minimum Description length of curve to be considered as lineament	0–8192 (pixel)
FTHR	Line Fitting error Threshold: It specifies the maximum error (in pixels) allowed in fitting a polyline to a pixel curve	0–8192 (pixel)
ATHR	Angular difference Threshold: It is the maximum angle between two vectors for them to be linked.	0–90 (degrees)
DTHR	Linking Distance Threshold: It specifies the minimum distance between the end points of two vectors for them to be linked.	0–8192 (pixel)

To extract automatically lineaments using PCI Geomatica, we tested some values for the six parameters of the Line module to see which would present the best result. In the end, all default values of these parameters were retained except GTHR revised to 60 pixels and ATHR to 35° as shown in Table 2.

Table 2. Default and verified values of Line module parameters

Parameters	Default Values	Verified Values
RADI	10	10
GTHR	100	**60**
LTHR	30	30
FTHR	3	3
ATHR	30	**35**
DTHR	20	20

The lineament extraction method used in this work being semi-automated, the automatic extraction was completed by manual editing using ArcGIS 10.8 software, with the objective of selecting or digitizing only the lineaments that can provide information on the geological structures of the study area (Figures 7 and 8).

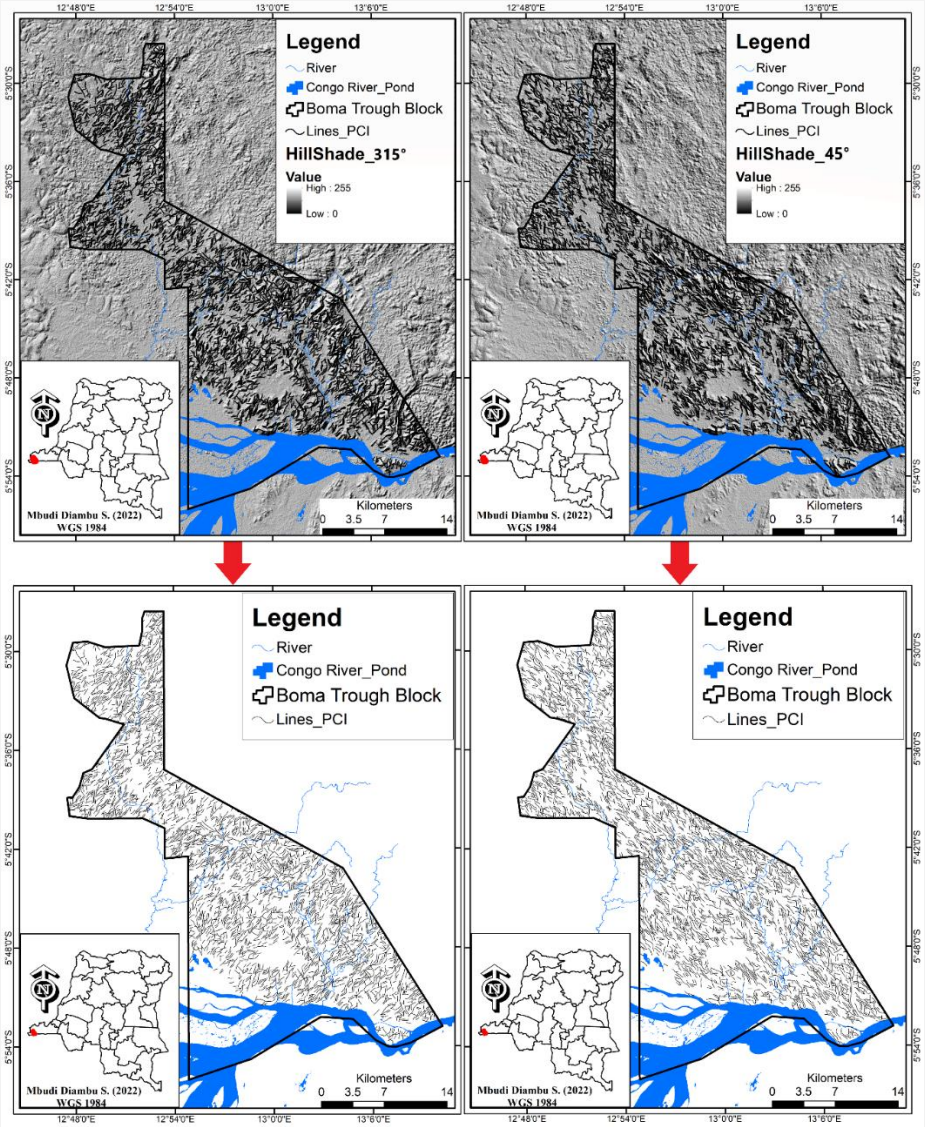

Figure 7. Map of lineaments extracted from traditional hillshade images (Azimuths 315° and 45°)

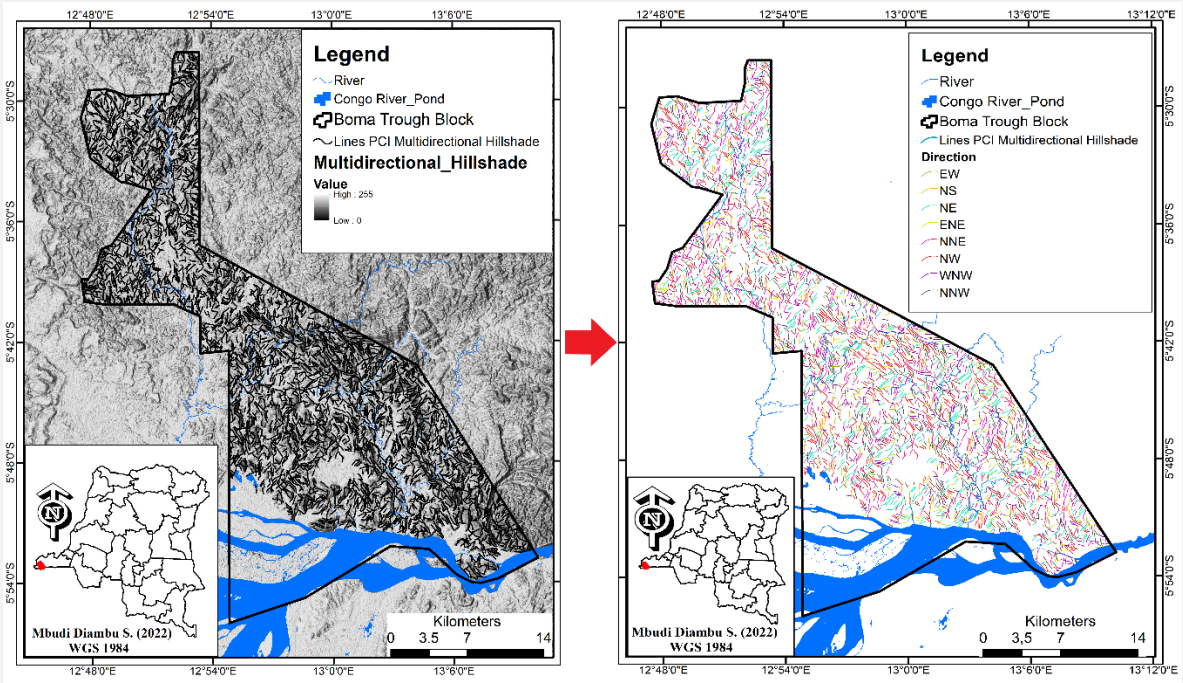

Figure 8. Map of lineaments extracted from multidirectional hillshade image

Statistical analysis of the extracted lineaments

The statistical analysis allowed to list all lineaments extracted semi-automatically on the traditional and multidirectional hillshade images. Table 3 below presents some basic statistical parameters (number, maximum length, minimum length, mean, standard deviation and total length of all lineaments). In all cases, the shortest lineament measures 0.16 km and the longest 3.79 km.

Table 3. Default and verified values of Line module parameters

	Traditional hillshade		
	Azimuth 315°	Azimuth 45°	Multidirectional hillshade
Number of lineaments	2688	2699	3129
Max length (km)	3.79	3.74	3.58
Min length (km)	0.19	0.16	0.17
Mean length (km)	0.699	0.697	0.667
Std. Dev. (km)	0.35	0.35	0.30
∑ length (km)	1877.86	1880.18	2087.82

Lineament rose diagram

The criterion used to differentiate families of lineaments according to the spatial direction was determined automatically with ArcGIS 10.8 from the coordinates of the lineament limits from the equation (Rebai et al., 2005):

$$\tan \alpha = \frac{|X_{end} - X_{start}|}{|Y_{end} - Y_{start}|} \quad (1)$$

With X_{end} and X_{start} the respective longitudes (in m) of lineament limits, Y_{end} and Y_{start} the latitudes (in m) of their limits, α the measurement of the angle expressed in degrees.

The dominant directions of the lineaments were indicated using the Rockworks 17 software. This allowed us to present the rose diagram of lineaments extracted from the hillshade images (Azimuths 315° and 45°) and multidirectional hillshade. Rose diagrams were produced by frequency in number (a) and cumulative length (b) of lineaments in the study area (Figure 9).

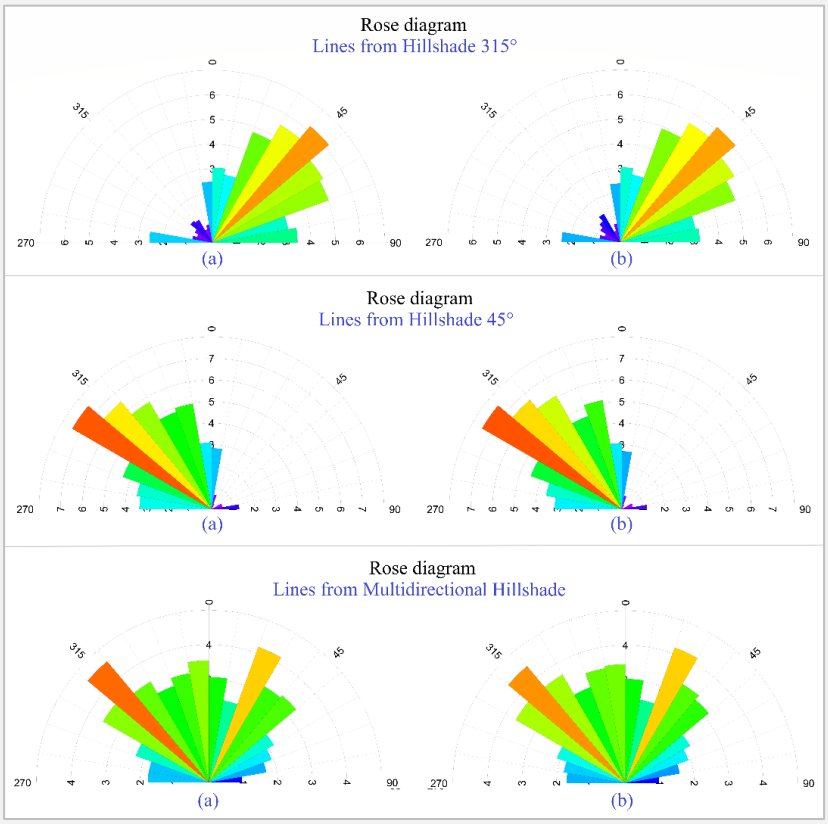

Figure 9. Rose diagram of lineaments extracted from traditional hillshade images (315° and 45° azimuths) and multidirectional (a - the frequency in number of lineaments and b - the frequency in cumulative length of lineaments)

From the rose diagrams above, we can note the following:

- The hillshade image with an azimuth of 315° allows to extract lineaments oriented preferentially in the NE-SW direction, with a weak influence towards the NW-SE;
- The hillshade of 45° azimuth presents lineaments oriented for the most part in the NW-SE direction, with a weak influence towards the NE-SW and
- The multidirectional hillshade image, which considers sunlight coming from several directions, allow to visualize as many lineaments as possible and shows that the dominant direction of lineaments is NW-SE, followed by NE-SW (NNE-SSW).

Lineament Directional Histograms

According to their orientations in space, the lineaments extracted from the three hillshade images (Figures 7 and 8) can be distributed in length, number and percentage as follows (Table 4):

Table 4. Distribution of lineaments in length, number and percentage according to their spatial orientations

Hillshade Azimuth 315°						
Length (km)	Number		%		Direction	
0.368-2.233	82		3.1		E-W	
0.310-1.577	151		5.6		N-S	
0.250-3.638		676		25.1		NNE
0.188-3.788		1150		42.8		NE
0.221-1.991	2120	294	78.9	10.9	NE	ENE
0.295-1.932		149		5.5		NNW
0.296-2.847		91		3.4		NW
0.289-2.278	335	95	12.5	3.5	NW	WNW
Total	2688		100			

Hillshade Azimuth 45°						
Length (km)	Number		%		Direction	
0.375-1.357	71		2.6		E-W	
0.352-1.929	136		5.0		N-S	
0.191-1.339		112		4.2		NNE
0.378-0.924		20		0.7		NE
0.221-1.509	195	63	7.2	2.3	NE	ENE
0.164-3.737		776		28.8		NNW
0.164-3.211		1130		41.9		NW
0.173-2.366	2297	391	85.1	14.5	NW	WNW
Total	2699		100			
Multidirectional hillshade						
Length (km)	Number		%		Direction	
0.375-0.927	44		1.4		E-W	
0.375-2.711	229		7.3		N-S	
0.166-3.575		642		20.5		NNE
0.205-2.206		537		17.2		NE
0.184-1.655	1360	181	44.1	5.8	NE	ENE
0.217-2.267		593		19.0		NNW
0.171-2.235		663		21.2		NW
0.218-2.357	1496	240	47.1	7.7	NW	WNW
Total	3129		100			

The histograms showing the distribution of the lineaments extracted according to their lengths, numbers and directions are presented in Figure 10 below.

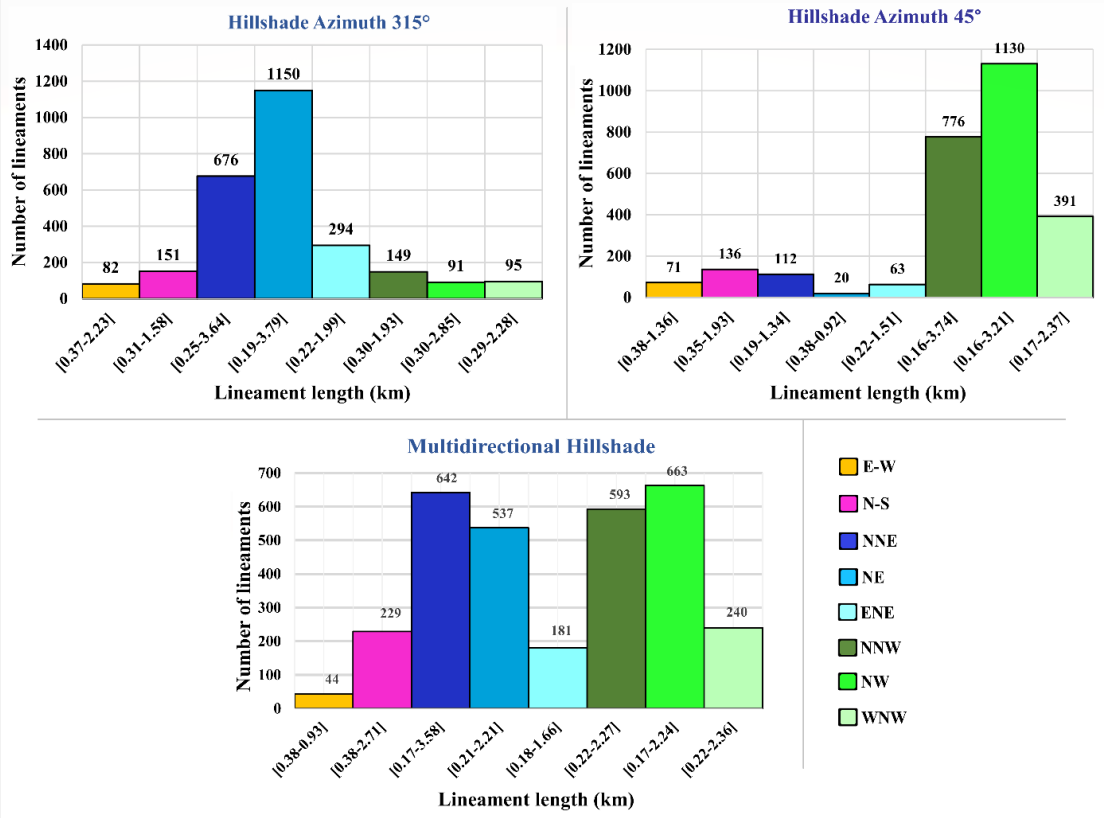

Figure 10. Directional histograms of extracted lineaments

Lineament density map

The density of lineaments is defined as the ratio of the total number of lineaments digitized by the surface of the zone considered (Edet et al., 1994). The lineament map is analyzed according to the different geological units of the region in order to calculate, for each of them, a density of lineaments from the ratio:

$$\text{Lineament density} = \frac{\text{Cumulative length of the lineaments (in km)}}{\text{Mapped area (in km}^2\text{)}} \quad (2)$$

In order to get an idea about the influence of tectonic stresses that deformed the study area, we mapped the density of lineaments using the "Line Density" command included in Spatial Analyst Tools of ArcGIS. Figures 11 and 12 below show lineament density maps in km/km² respectively for traditional and multidirectional hillshade images.

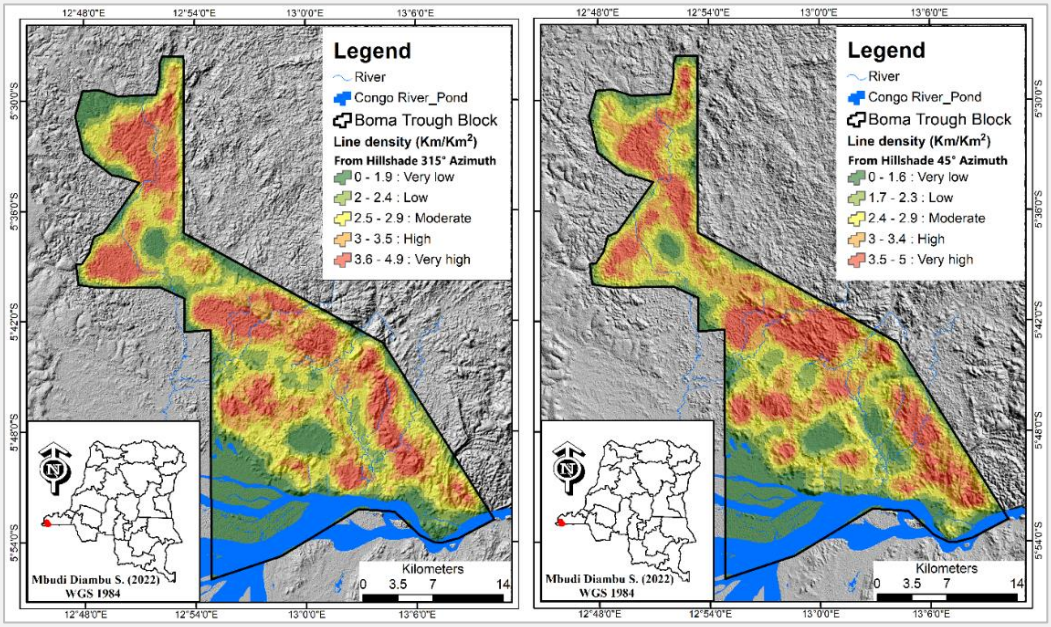

Figure 11. Density of lineaments extracted from traditional hillshade (Azimuths 315° and 45°)

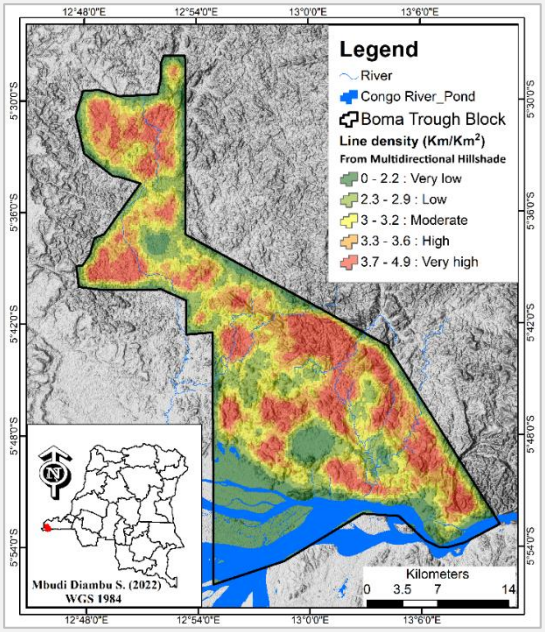

Figure 12. Density of lineaments extracted from multidirectional hillshade

By observing the maps above, we find that the lineament density values vary from 0 to 5 Km/Km², divided into five classes for each map, ranging from very low, low, moderate, high to very high density. The areas covered by density class are presented in km² and in percentage (Table 5), for a total area of the study area of 747 km².

Table 5. Areas covered by each lineament density class

		Hillshade Azimuth 315°		Hillshade Azimuth 45°		Multidirectional Hillshade	
		Area		Area		Area	
Class	Density Level	Km²	%	Km²	%	Km²	%
Class 1	Very low	190	25	162	22	181	24
Class 2	Low	99	13	118	16	125	17
Class 3	Moderate	143	19	160	21	120	16
Class 4	High	168	22	153	20	157	21
Class 5	Very high	147	20	154	21	164	22
∑Area		747	100	747	100	747	100

Validation of lineaments in the field

To confirm the presence of geological and morphostructural lineaments in our study area, we carried out a field trip in Boma Trough Block for a period of two weeks in search of data to validate the results obtained from the processing of data by remote sensing. The idea behind this step is to physically see lineaments related to the morphology and geological structures of the study area, which can be recognized in situ and have geological significance. The lineaments recognized in the field have been validated on the hillshade multidirectional model for the simple reason that it takes into account all azimuths of the light source as mentioned above and allow to detect many lineaments.

In this context, our campaign was carried out along five geological cross-sections (Figure 13), all oriented North-East/South-West and perpendicular to the direction of most of lineaments extracted from the hillshade multidirectional model. This allowed us to validate on the field 112 lineaments (faults, rock outcrops, lithological limits, axes of folds, valleys, rivers, etc.) among the 3129 extracts from the image. The number of lineaments validated represents only 3.6% of all lineaments extracted, an addition of geological cross-sections would be necessary and would allow to confirm more lineaments in the field.

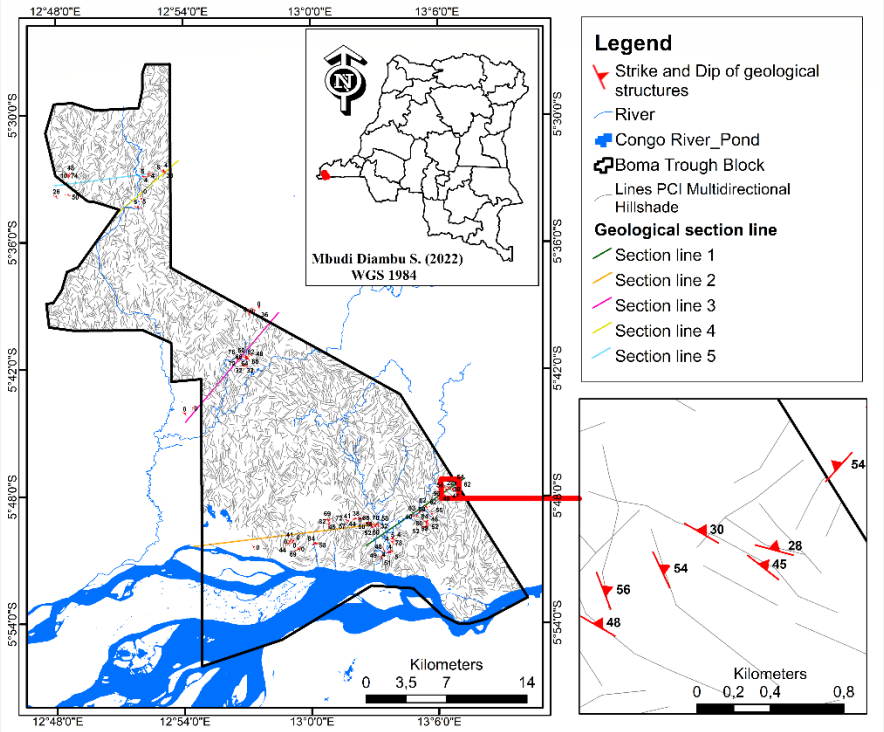

Figure 13. Map of geological section lines and sites of structural measurements in the field

Illustration of some field observation sites

As mentioned above, 112 lineaments among those extracted from the multidirectional hillshade image were validated in the field, observed at different sites, among which we have, for illustrative purposes, the seven (7) below (Figure 14):

- *Site A11:* Located in an artisanal stone-pit in the west of Boma city, at coordinates 13°5'26.6"E and 5°49'23.7"S, we note the presence of a geological lineament validated on a quartzitic formation, in monoclinal structure with direction N132° and dip 80°SW;
- *Site A25:* located in the east of Boma, at coordinates 13°2'48.4"E and 5°49'21.4"S, the site has a validated geological lineament on a migmatitic formation, direction N153°, affected by a normal fault of approximately 5.5 dm of deplacement with tectoglyphs clearly visible to the eye, with direction N63°E and dip 68°NE;
- *Site A31:* at coordinates 13°2'1.8"E and 5°49'3.5"S and located to the east of Boma, we have the presence of a validated geological lineament on a migmatitic formation with a massive and elongated aspect along the N135° direction;
- *Site A57:* located at coordinates 13°3'49.4"E and 5°50'0.2"S, about 3km at the north of Congo River, visible on the left shore of Kalamu River, we note the presence of a geological lineament validated on a tabular sedimentary formation (alternation between sandstone and limestone), direction N105° and dip 4°SW, affected by a normal fault plunging at 78° towards the SW with a deplacement of approximately 0.3 meter;
- *Site B04:* located along the Khoko Khandu river about 1.4 km from the village Khandu Lemba, at coordinates 12°56'57.9"E and 5°41'27.6"S, we note the presence of a lineament geological validated on a quartzite formation outcrop in a monoclinal structure following the direction N113° and a dip of 64°SW;
- *Site B05:* at coordinates 12°56'57.2"E and 5°41'24.8"S, we have a validated geological lineament on an outcrop of quartzite in monoclinal structure with direction N108° and dip 62°SW, crossed by a vertical fault trending N25°E and followed by the Khoko Khandu river;
- *Site D02:* Located about 1 km of the Mavuma oil sands block, at coordinates 12°48'32.7"E and 5°32'46.6"S, a lineament has been validated on a limestone formation impregnated by crude oil, direction N74°E/dip 15°NW.

Figure 14. Illustration of some sites of structural measurements in the field

Rose diagram et Wulff stereonet diagram

The analysis of relationships between directional data has been greatly facilitated by the use of iso-angle (Wulff stereonet) and iso-surface (Schmidt stereonet) projection methods. As a result, the stereonet has been established as the most fundamental tool for the structural geologist (Knox-Robinson & Gardoll, 1998).

Based on the structural measurements (strike and dip) of the lineaments observed in the field, a rose diagram and stereonet diagram (Wulff Net) were produced using the Rockworks 17 software, showing a dominant NW-SE orientation of the lineaments, followed by NE-SW, as shown in Figure 15 below.

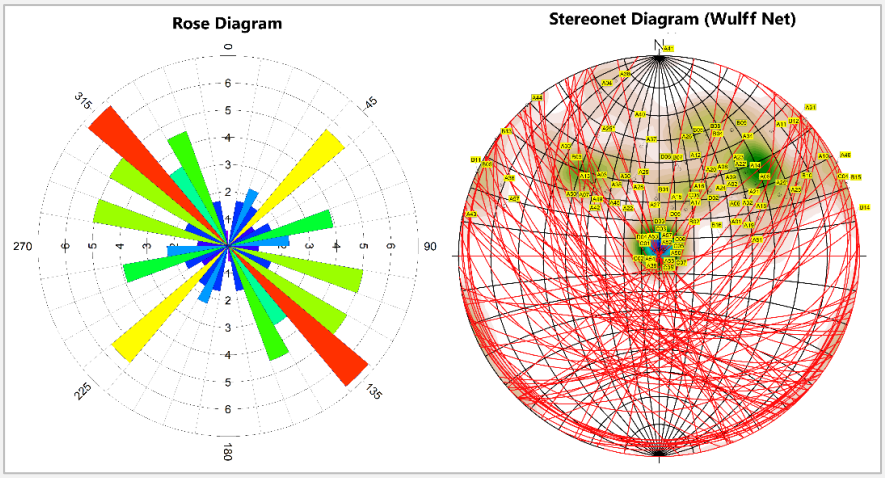

Figure 15. Rose diagram and Stereonet diagram (Wulff Net) of structural field measurements

DISCUSSION

The analysis of the hillshade images presented in this work shows that the multidirectional hillshade method allowed to better extract the lineaments in the study area compared to the traditional hillshade method.

By comparing the rose diagram of the lineaments extracted from the multidirectional hillshade image (Figure 9) with that of the lineaments validated in the field (Figure 15), we can note some similarity in terms of lineament orientation. Which means that for both cases, the dominant orientation of the lineaments is NW-SE, followed by NE-SW. However, it is normal to note small differences between the rose diagrams of these two cases, given that the lineaments validated in the field represent only a sample of those extracted from the satellite image and also as a result of errors that may occur during the process of semi-automatic extraction of the lineaments.

The orientations of lineaments as presented in this study correspond exactly to the results of the work of Kalala-Ntumba et al. (1975) who confirm the NW-SE orientation of the western and eastern Precambrian hills of Boma as well as those of Giresse (1982) mentioning moderate but fairly dense folds in the Congolese Coastal Basin, affecting the Upper Cretaceous and Paleogene geological formation, to the middle Eocene and oriented NW-SE. Nsungani (2012) mentions that the structures (anticlines and synclines) in the northwestern part of Angola (or south of our study area), draw a virgation, oriented NNW-SSE. This NW-SE orientation of lineaments would probably be due to tectonic stresses related to the opening of the South Atlantic at the beginning of the Cretaceous.

The alignment of some lineaments around Boma oriented NE-SW would be the expression of some Precambrian faults, followed by the Congo River and some of its tributaries in the region as asserted by Kalala-Ntumba et al. (1975) and Streenstra (1988). Similar fault lateral movements have been suggested in neighboring countries, interpreted either as reactivated Precambrian basement trends or as onshore extensions of Atlantic transform faults (Gaffney et al., 1988). The structural context of Boma Trough Block is therefore dependent on that of the Congolese Coastal Basin where it is located.

In addition, the three lineament density maps developed reveal almost the same density pattern in places. By comparing the lineament density map from the multidirectional hillshade image (Figure 12) to the geological map of the study area (Figure 2), we can note that the large part of low and very low density areas (0 to 2.9 Km/Km^2) corresponds to sedimentary environments (modern alluvium of the Holocene or sandstone/limestone/argillite of the continental lower Cretaceous), covering an area of

around 306 km² while the high and very high density zones (3.3 to 4.9 Km/Km²) contain the formations of the Precambrian basement and cover an area of 321 Km².

Which means that most of our study area would have been deformed by strong tectonic stresses. The various fractures (faults) observed on the basement would have preceded the deposition of the sediments. However, the normal fault observed in a sedimentary environment at site A57 (Figure 14) would be the expression of an active fault in the basement after deposition of sediments or the consequence of an underground cavity.

It is also useful for us to note the presence of high densities of lineaments in some sedimentary zones to the west of the block. These areas are interesting for oil research because the tectonic stresses allow the installation of oil traps in a sedimentary basin. It is therefore possible with more appropriate prospecting methods such as seismic to locate these traps at depth. It is therefore possible with more appropriate prospecting methods such as seismic to locate these traps at depth. Oil seepage in a high-density zone, as discovered at site D02 (Figure 14), would have followed geological lineaments (faults or fractures) and would indicate the presence of a petroleum deposit underneath, which geophysical methods would allow to locate.

According to Asadzadeh & de Souza Filho (2017), surface manifestations of oil and gas can be divided into two categories, namely macro and micro-seepage. Macro-seepage is the surface expression of a leakage path, usually related to tectonic discontinuities, along which oil or natural gas flows from a subterranean source (Link, 1952; Clarke & Cleverly, 1991; Macgregor, 1993). Micro-seepage, refers to the slow, invisible but present migration of light alkanes (C1 - C5) and volatiles from accumulation to the surface (Etiope, 2015; Price, 1986; Schumacher, 1999). Micro-seepage is not linked to faults, but it can be reinforced by the presence of faults and large fractures (Richers et al., 1982).

CONCLUSION

This work consisted of an analysis of the structural context of Boma Trough Block, which is an oil block located in the onshore of the Coastal Basin of D.R. Congo, based essentially on the study of the geological and morphostructural lineaments resulting from the processing of an ALOS PALSAR DEM satellite image.

The ALOS PALSAR DEM image used, with a spatial resolution of 12.5 m, was enhanced using traditional (Azimuths 45° and 315°) and multidirectional hillshade methods, in order to better visualize lineament trends in the study area. The extraction of the lineaments was done semi-automatically, by combining the contribution of GIS and remote sensing software and the appreciation of the operator. This allowed us to extract 2688 lineaments for the 315° azimuth hillshade image, 2699 for the 45° azimuth one and 3129 for the multidirectional hillshade image. The shortest lineament extracted presented a length of 0.16 km and the longest was 3.79 km.

The hillshade image of azimuth 315° allowed to extract lineaments oriented for the most part in the NE direction and that of 45° for the NW direction. The multidirectional hillshade image for its part showed that taking into account all the azimuths, the dominant direction of the lineaments in Boma Trough Block is NW (representing 47.1% of lineaments), followed by NE (44, 1%), N-S (7.3%) and E-W (with 1.4%). To better visualize this reality, rose diagrams and directional histogram graphs have been established based on the orientation, number and length of the lineaments extracted.

In order to get an idea of the impact of tectonics in the study area, we have developed lineament density maps for all extracted lineament maps. The density maps showed values ranging from 0 to 5 Km/Km², divided into five classes, ranging from very low, low, moderate, high and very high density values.

Analysis of the lineament density map from the multidirectional hillshade image revealed that the high and very high density areas covered an area of 321 km² or 43% of the area of the study area (including mainly the Precambrian basement), 306 km² or 41% for areas with low and very low densities (mostly covering sedimentary formations) and 120 km² or 16% for areas with moderate density.

In order to evaluate the contribution of the processing approach used in this work, the lineaments extracted from the ALOS PALSAR DEM image have been confronted with the realities on the field and have shown a positive correlation. The results found were conclusive and satisfactory, useful for the research of petroleum deposits.

REFERENCES

Ablin, R., Sulochana, C. H., & Prabin, G. (2020). An investigation in satellite images based on image enhancement techniques. *European Journal of Remote Sensing, 53*(sup2), 86-94. https://doi.org/10.1080/22797254.2019.1673216

Ahmadi, H., & Pekkan, E. (2021). Fault-based geological lineaments extraction using remote sensing and GIS—a review. *Geosciences, 11*(5), 183. https://doi.org/10.3390/geosciences11050183

Asadzadeh, S., & de Souza Filho, C. R. (2017). Spectral remote sensing for onshore seepage characterization: A critical overview. *Earth-Science Reviews, 168*, 48-72. https://doi.org/10.1016/j.earscirev.2017.03.004

Aziz, K. M. A., & Rashwan, K. S. (2022). Comparison of different resolutions of six free online DEMs with GPS elevation data on a new 6th of October City, Egypt. *Arabian Journal of Geosciences, 15*(20), 1585. https://doi.org/10.1007/s12517-022-10845-5

Bellion, Y., & Guiraud, R. (1980). Tectonique intraplaque : mise en évidence sur le littoral sénégalais de déformations liées à la phase tectorogène pyrénéo-atlasique. *8e Réun. Ann. Sei. Terre, Marseille*, p. 33.

Benkhelil, J., & Guiraud, R. (1980). La Bénoué (Nigria): une chaîne intra-continentale de style atlasique. *8e Réun. Ann. Sei. Terre, Marseille*, p. 37.

Clarke, R. H., & Cleverly, R. W. (1991). Petroleum seepage and post-accumulation migration. *Geological Society, London, Special Publications, 59*(1), 265-271. https://doi.org/10.1144/GSL.SP.1991.059.01.17

Das, S., Pardeshi, S. D., Kulkarni, P. P., & Doke, A. (2018). Extraction of lineaments from different azimuth angles using geospatial techniques: a case study of Pravara basin, Maharashtra, India. *Arabian Journal of Geosciences, 11*(8). doi:10.1007/s12517-018-3522-6

Echeverria, M. D. P. V., Ortega, A. G. V., Larreta, E., Crespo, P. R., & Mulas, M. (2022). Lineament Extraction from Digital Terrain Derivate Model: A Case Study in the Girón–Santa Isabel Basin, South Ecuador. *Remote Sensing, 14*(21), 5400. https://doi.org/10.3390/rs14215400

Edet, A. E., Teme, S. C., Okereke, C. S., & Esu, E. O. (1994). Lineament analysis for groundwater exploration in Precambrian Oban massif and Obudu plateau, SE Nigeria. *Journal of Mining and Geology, 30*(1), 87-95.

Etiope, G. (2015). *Natural Gas Seepage: The Earth's Hydrocarbon Degassing*. Springer International Publishing, Switzerland. https://doi.org/10.1007/978-3-319-14601-0

Gaffney, Cline & Associates. (1988). *Etude sur les réserves du Bassin Littoral de la République du Zaïre. Aspects géologiques régionaux et prospects d'exploration vue d'ensemble des facilités et ensemble des données.* Département des Mines et Energie du Zaïre.

Giresse, P. (1982). La succession des sédiments dans les bassins marins et continentaux du Congo depuis le début du Mésozoïque. *Sciences Géologiques, bulletins et mémoires, 35*(4), 183-206. https://doi.org/10.3406/sgeol.1982.1620

Guoan, T. (2014). Progress of DEM and digital terrain analysis in China. *Acta Geographica Sinica, 69*(9), 1305–1325. https://doi.org/10.11821/dlxb201409006

Hobbs, W. H. (1904). Lineaments of the Atlantic border region. *Bulletin of Geological Society of America, 15*(1), 483-506. https://doi.org/10.1130/GSAB-15-483

Jansen, J. H. F., Giresse, P., & Moguedet, G. (1984). Structural and sedimentary geology of the Congo and Southern Gabon continental shelf; a seismic and acoustic reflection survey. *Netherlands Journal of Sea Research, 17*(2-4), 364-384. https://doi.org/10.1016/0077-7579(84)90056-5

Kalala-Ntumba, A. K., Keesmann, I., Grzybowski, K. (1975). *Carte géologique s 6/13-sw 3a boma (bas-zaïre).* Presses universitaires du Zaïre.

Khal, M., Algouti, A., Algouti, A., Akdim, N., Stankevich, S. A., & Menenti, M. (2020). Evaluation of open Digital Elevation Models: estimation of topographic indices relevant to erosion risk in the Wadi M'Goun watershed, Morocco. *AIMS Geosciences, 6*, 231-257. https://doi.org/10.3934/geosci.2020014

Knox-Robinson, C. M., & Gardoll, S. J. (1998). GIS-stereoplot: an interactive stereonet plotting module for ArcView 3.0 geographic information system. *Computers & Geosciences, 24*(3), 243–250. https://doi.org/10.1016/S0098-3004(97)00122-2

Le Pichon, X. (1968). Sea-floor spreading and continental drift. *Journal of geophysical research, 73*(12), 3661-3697. https://doi.org/10.1029/JB073i012p03661

Lepersonne, J. (1974). *Notice explicative de la carte géologique du Zaïre au 1/2000.000*. République du Zaïre, Département des mines, Direction de la Géologie, Kinshasa, 67p.

Link, W. K. (1952). Significance of oil and gas seeps in world oil exploration. *AAPG Bulletin, 36*(8), 1505-1540. https://doi.org/10.1306/5CEADB3F-16BB-11D7-8645000102C1865D

Lu, P. F., & An, P. (1999). A metric for spatial data layers in favorability mapping for geological events. *IEEE transactions on geoscience and remote sensing, 37*(3), 1194-1198. https://doi.org/10.1109/36.763271

Macgregor, D. S. (1993). Relationships between seepage, tectonics and subsurface petroleum reserves. *Marine and Petroleum Geology, 10*(6), 606–619. https://doi.org/10.1016/0264-8172(93)90063-X

Masoud, A. A., & Koike, K. (2011). Auto-detection and integration of tectonically significant lineaments from SRTM DEM and remotely-sensed geophysical data. *ISPRS Journal of Photogrammetry and Remote Sensing, 66*(6), 818–832. https://doi.org/10.1016/j.isprsjprs.2011.08.003

Minár, J. & Sládek, J. (2009). Morphological network as an indicator of a morphotectonic field in the central Western Carpathians (Slovakia). *Zeitschrift Für Geomorphologie, Supplementary Issues, 53*(2), 23–29. https://doi.org/10.1127/0372-8854/2009/0053S3-0023

Ministère des Hydrocarbures (2022*). Atlas des Blocs pétroliers et Gaziers de la République Démocratique du Congo, 1ère Phase des Appels d'Offres.*

MRAC. (2005). *Carte Géologique au 1:2500000 de la République Démocratique du Congo. Tervuren.*

MRAC. (2010). *Carte géologique au 1: 500.000 de la République Démocratique du Congo, Province du Kongo Central, Tervuren.*

Nagi, R. (2014). *Multidirectional Hillshade Makes Your Maps Pop.* Environmental Systems Research Institute (ESRI). https://www.esri.com/~/media/files/pdfs/news/arcuser/1014/multi-directional-hillshade-makes-your-maps-pop.pdf

Nsungani, P. C. (2012). *La chaine panafricaine du Nord-Ouest de l'Angola: Etude pétrostructurale, géochimique et géochronologique. Implications géodynamiques* (Doctoral dissertation, Montpellier 2).

O'leary, D. W., Friedman J. D., Pohn, H. A. (1976). Lineament, linear, lineation: Some proposed new standards for old terms. *Geological Society of America Bulletin, 87*, 1463-1469. https://doi.org/10.1130/0016-7606(1976)87%3C1463:LLLSPN%3E2.0.CO;2

Pal, S. K., Majumdar, T. J., & Bhattacharya, A. K. (2006). Extraction of linear and anomalous features using ERS SAR data over Singhbhum Shear Zone, Jharkhand using fast Fourier transform. *International Journal of Remote Sensing, 27*(20), 4513–4528. https://doi.org/10.1080/01431160600658172

Prasad, A. D., Jain, K., & Gairola, A. (2013). Mapping of lineaments and knowledge base preparation using geomatics techniques for part of the Godavari and Tapi basins, India: A case study. *International Journal of Computer Applications, 70*(9). https://doi.org/10.5120/11994-7875

Price, L. C. (1986). A critical overview and proposed working model of surface geochemical exploration. In *Unconventional methods in exploration for petroleum and natural gas*. Southern Methodist University Press, Dallas, pp. 245–304.

Rebai, N., Mabrouk, Y., B. & Bouaziz, S. (2005). Elaboration d'un SIG intégrant des modèles de représentation relatifs aux données géologiques et structurales du Sahel de Sfax. *Annales des Mines et de la Géologie, 43*, 37-56.

Richers, D. M., Reed, R. J., Horstman, K. C., Michels, G. D., Baker, R. N., Lundell, L., & Marrs, R. W. (1982). Landsat and soil-gas geochemical study of Patrick Draw oil field, Sweetwater County, Wyoming. *AAPG Bulletin, 66*(7), 903-922. https://doi.org/10.1306/03B5A354-16D1-11D7-8645000102C1865D

Salui, C. L. (2018). Methodological Validation for Automated Lineament Extraction by LINE Method in PCI Geomatica and MATLAB based Hough Transformation. *Journal of the Geological Society of India, 92*(3), 321–328. https://doi.org/10.1007/s12594-018-1015-6

Scanvic, J. Y. (1983*). Utilisation de la télédétection dans les sciences de la terre*. Manuels et méthodes-Bureau de recherches géologiques et minières, (7).

Scheiber, T., Fredin, O., Viola, G., Jarna, A., Gasser, D., & Łapińska-Viola, R. (2015). Manual extraction of bedrock lineaments from high-resolution LiDAR data: methodological bias and human perception. *Gff, 137*(4), 362-372. https://doi.org/10.1080/11035897.2015.1085434

Schumacher, D. (1999). *Surface Geochemical Exploration for Petroleum*. Handbook of Petroleum Geology : Exploring for Oil and Gas Traps. AAPG, Tulsa, OK.

Streenstra, B. (1988). La géomorphologie du Bas-Zaïre. *Symposium L'Accès maritime au Zaïre, Bruxelles, 5 Déc. 1988. Académie Royale des Sciences d'Outre-Mer*, pp. 21-42.

Suzen, M. L., & Toprak, V. (1998). Filtering of satellite images in geological lineament analyses: An application to a fault zone in Central Turkey. *International Journal of Remote Sensing, 19*(6), 1101–1114. https://doi.org/10.1080/014311698215621

Ustinov, S., Ostapchuk, A., Svecherevskiy, A., Usachev, A., Gridin, G., Grigor'eva, A., & Nafigin, I. (2022). Prospects of Geoinformatics in Analyzing Spatial Heterogeneities of Microstructural Properties of a Tectonic Fault. *Applied Sciences, 12*(6), 2864. https://doi.org/10.3390/app12062864

William, B. (2018). *ArcGIS for Environmental and Water Issues*. Springer. https://doi.org/10.1007/978-3-319-61158-7